Novel Atmospheric Growth Technique to Improve Both Light Absorption and Charge Collection in ZnO/Cu_2O Thin Film Solar Cells

*Andrew T. Marin, David Muñoz-Rojas, Diana C. Iza, Talia Gershon, Kevin P. Musselman, and Judith L. MacManus-Driscoll**

In low temperature grown ZnO/Cu_2O solar cells, there is a discrepancy between collection length and depletion width in the Cu_2O which makes the simultaneous achievement of efficient charge collection and high open-circuit voltage problematic. This is addressed in this study by fabricating ZnO/Cu_2O/Cu_2O^+ back surface field devices using an atmospheric atomic layer deposition (AALD) printing method to grow a sub-200-nm Cu_2O^+ film on top of electrodeposited ZnO and Cu_2O layers. The AALD Cu_2O^+ has a carrier concentration around 2 orders of magnitude higher than the electrodeposited Cu_2O, allowing the electrodeposited Cu_2O layer thickness in a back surface field cell to be reduced from 3 μm to the approximate charge collection length, 1 μm, while still allowing a high potential to be built into the cell. The dense conformal nature of the AALD layer also blocks shunt pathways allowing the voltage enhancement to be maintained. The thinner cell design reduces recombination losses and increases charge collection from both incident light and light reflected off the back electrode. Using this design, a short circuit current density of 6.32 mA cm^{-2} is achieved–the highest reported J_{SC} for an atmospherically deposited ZnO/Cu_2O device to date.

1. Introduction

Nontoxic, earth-abundant solar absorbers have gained increasing attention for use in safe, inexpensive, and renewable electricity generation.[1] The ZnO/Cu_2O system, for example, is comprised of inexpensive metal-oxide semiconductors,[1,2] has a high theoretical efficiency of 10–20%,[3–5] and can be fabricated using low-cost, scalable, atmospheric methods such as electrochemical deposition.[3,6–8]

However, common to many solution-processed inorganic systems, electrodeposited (ED) ZnO/Cu_2O cells experience a number of fundamental limitations.[9] Particularly detrimental is the discrepancy between the charge collection length (<1 μm) and depletion width (up to 3 μm) in the Cu_2O, which results from the combination of a short electron transport length (mainly due to a small electron mobility in Cu_2O)[10] and low hole concentration.[5,10–12] These factors produce a recombination region at distances far (>1 μm) from the heterojunction interface in the Cu_2O where the minority carriers recombine before reaching the junction and hence do not contribute to the resulting current density.

Previous research has addressed the limited collection length by nanostructuring the interface to reduce the required minority carrier transport length.[10] In another approach the Cu_2O layer thickness was reduced to the charge collection length at the same time as implementing a low refractive index polymer.[5] These cells exhibited optical confinement[5,13,14] wherein unabsorbed photons (particularly longer phonon-coupled wavelengths)[15,16] were reflected back into the collection region of the Cu_2O and absorbed near the junction. However, in both of the above cases, while the short circuit current densities were increased by ~15% in both cells (to 4.6–5.3 mA cm^{-2}), the devices displayed low open circuit voltages (V_{OC}) of less than 0.3 V due to inhibited formation of the depletion layer in the Cu_2O.[5,10] Thus in atmospherically processed ZnO/Cu_2O devices the challenge remains to maximize *both* charge collection and voltage output.

With the aim of increasing the V_{OC}, research has focused on doping Cu_2O to make it more heavily p-type to decrease the depletion width and allow the full built-in potential to be realized in a thickness commensurate with the electron collection length. However, p-type doping of Cu_2O has given limited results thus far, particularly under atmospheric conditions.[17–23]

Other photovoltaic systems have utilized a back-surface-field (BSF) design where subsequent layers (moving away from the p-n junction) are highly-doped to create a graded structure.[24–28] BSF cells have yielded higher V_{OC}[27,28] by reducing the recombination velocity of minority carriers and by drawing the

A. T. Marin, Dr. D. Muñoz-Rojas, Dr. D. C. Iza, Dr. T. Gershon, Prof. J. MacManus-Driscoll
Department of Materials Science and Metallurgy
University of Cambridge
Pembroke St., Cambridge CB2 3QZ, UK
E-mail: jld35@cam.ac.uk
Dr. K. P. Musselman
Cavendish Laboratory
University of Cambridge
Cambridge, UK

DOI: 10.1002/adfm.201203243

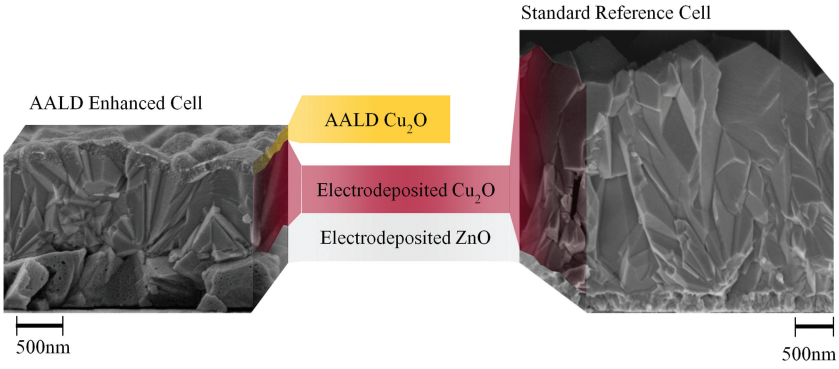

Figure 1. Cross section SEM images of an AALD-enhanced cell (left) and fully-ED reference cell (right). For the AALD-enhanced cell, 500 nm of ZnO was ED on ITO followed by 1 µm of ED Cu_2O and various thicknesses of AALD Cu_2O^+. For the fully-ED reference cell, 500 nm of ZnO was ED on ITO followed by 3 µm of ED Cu_2O.

carriers towards opposite electrodes. To our knowledge, there is only one reported theoretical study of using such a $n/p/p^+$ structure with a Cu_2O system and no experimental results have been reported thus far.[29] The lack of experimental results most likely stem from the limited ability to dope Cu_2O.

In this study, trilayer $ZnO/Cu_2O/Cu_2O^+$ devices were fabricated on ITO/glass substrates. The ZnO and Cu_2O layers were grown using electrochemical deposition and the Cu_2O^+ layer was grown by another atmospheric fabrication technique–atmospheric atomic layer deposition (AALD). AALD (also referred to as spatial ALD[30] or ultrafast ALD)[31] is a printing-type process that allows for up to an order of magnitude faster growth than traditional ALD.[30–34] The technique has recently been used as a viable means to deposit barrier layer films for photovoltaic devices,[32,35] but has not, so far, been shown to be applicable to the active layers in such devices.

Herein, we show that Cu_2O grown by AALD has a carrier concentration two orders of magnitude higher than films grown by electrodeposition, allowing us to produce a BSF cell with a short circuit current density (J_{SC}) of 6.32 mA cm^{-2}–the highest reported J_{SC} for an atmospherically deposited ZnO/Cu_2O device measured under standard AM1.5 illumination. By coating cells with a sub-200 nm AALD layer, the ED Cu_2O layer thickness can be reduced from 3 µm to approximately the charge collection length, 1 µm, while maintaining a high built in potential. Device measurements and modelling suggest that a strong electric field is created that drives carrier collection and minimizes losses in the recombination region. The thinner device structure should also give enhanced collection of charges from unabsorbed light reflecting off the back electrode, similar to how other types of solar cells have benefited from multiple-pass light.[36–38]

2. Results

2.1. Reducing the Cu_2O Thickness without Losing Built-in Potential: Carrier Concentrations and Cell Structure

The carrier concentration of an ED Cu_2O film was measured to be 6×10^{13} cm^{-3}. This provides a lower bound for the acceptor density and indicates that a Cu_2O film up to ~3 µm thick may be required to build in the full depletion width for a ZnO/Cu_2O heterojunction (for a 0.7 V built-in potential based on the estimated offset in Fermi levels of the ZnO, 4.2 eV, and Cu_2O, 4.9 eV, as depicted by the energy level diagram, Figure S1 in the Supporting Information).[5,8,39] Since the charge collection length of Cu_2O does not exceed 1 µm, the disparity in these length-scales produces a recombination region up to 2 µm thick where minority carriers from photons absorbed beyond the charge collection length cannot reach the ZnO/Cu_2O junction.

The carrier concentrations of the Cu_2O^+ films grown by AALD were measured to be $8.3 \pm 1.5 \times 10^{15}$ cm^{-3}–two orders of magnitude higher than the ED film. The reason for the higher carrier concentration is believed to be related to the growth of the Cu_2O closer to the CuO phase boundary giving a higher copper vacancy concentration induced by using relatively high oxidation conditions. XRD data confirming that the material is Cu_2O is given in the supporting information (Supporting Information Figure S2).

In this study, 1 µm of ED Cu_2O was used to produce the approximate charge collection length, and then a thin AALD Cu_2O^+ layer was deposited on top to build in a strong electric field to drive charges out of the device. **Figure 1** shows cross-sectional SEM images of both an AALD-enhanced cell (500 nm ED-ZnO/1 µm ED-Cu_2O/~200 nm AALD-Cu_2O^+) and a fully-ED 3 µm reference cell (500 nm-ZnO/3 µm ± 0.25 µm standard deviation -Cu_2O). Large columnar grains are observed in the ED layer and a dense, conformal coating is observed for the AALD film. The dense nature of the AALD film is expected to block pinholes and grain boundaries which act as shunt pathways in the underlying ED Cu_2O layer,[5] a point that we address in Section 2.2.

Figure 2 shows the energy level (Figure 2a,b) and electric field (Figure 2c) profile of the AALD-enhanced ZnO/Cu_2O(1 µm) p-n heterojunction with the additional $p\text{-}p^+$ junction compared to a fully-ED ZnO/Cu_2O(3 µm) reference cell. The profiles were calculated using the PC1D modelling software.[40] Similar results were obtained by hand calculation using the equations of Kuznicki et al.[41] As shown in Figures 2a,c, ~150 nm of AALD Cu_2O^+ is necessary to complete the full depletion width. This suggests that 150 nm of AALD Cu_2O^+ should be able to replace the ~2 µm recombination region of the 3 µm reference cell without deteriorating the built-in potential. Additionally, for the AALD-enhanced cell, we see a much higher electric field (Figure 2c) than in the 3 µm reference cell for all distances from the pn junction interface up to the final ~100 nm of the depletion region. Hence the improved electric field across the cell is due to the potential being accommodated across a smaller width in the Cu_2O, made possible by excess holes in the AALD Cu_2O^+ that diffuse into the ED layer.

The fairly-uniform electric field distribution, similar to a p-i-n device,[42] of the AALD-enhanced structure (Figure 2) is also expected to produce a larger collection length than the gradually

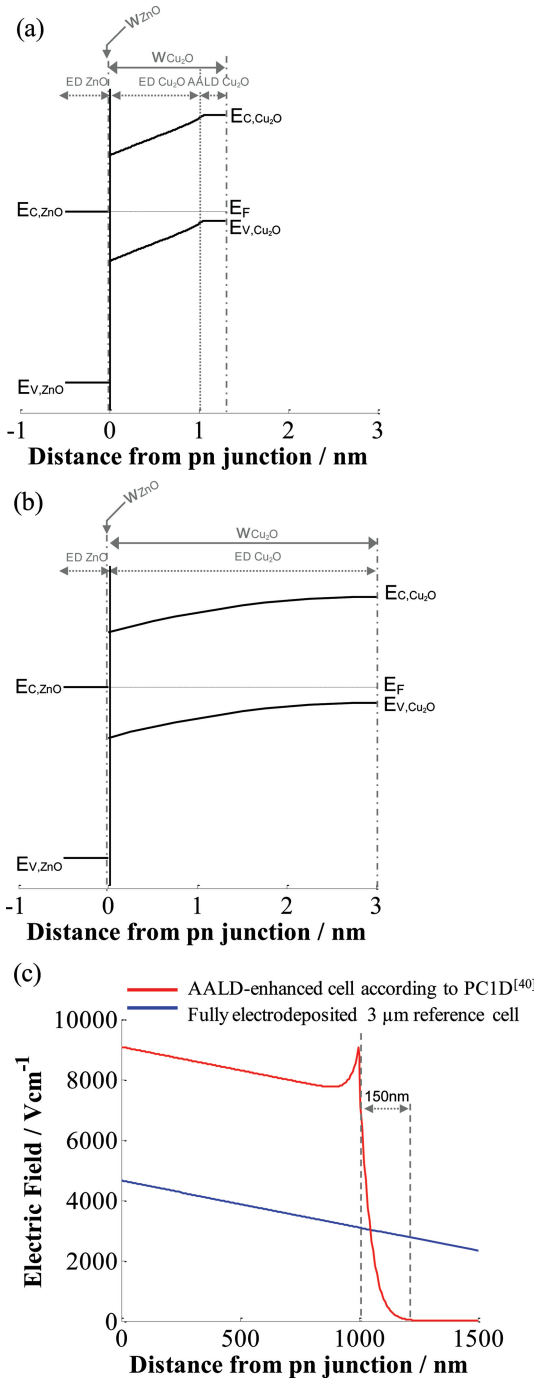

Figure 2. Band energy-displacement diagram for an a) AALD-enhanced and b) fully-ED reference cell. c) Predicted electric field on the p-side of the p-n junction for an AALD-enhanced cell calculated using the PC1D modelling software.[40] The AALD-enhanced electric field profile is compared to the field of a fully-ED 3 µm reference cell. Assumed values of parameters used for calculating the energy levels and electric field are: $\varepsilon_{ZnO} = 8\varepsilon_0$, $\varepsilon_{Cu2O} = 7\varepsilon_0$, $N_{D,ZnO} = 1 \times 10^{18}$ cm^{-3}, $N_{A,Cu2O,ED} = 6 \times 10^{13}$ cm^{-3}, $N_{A,Cu2O,AALD} = 8.3 \times 10^{15}$ cm^{-3}, $N_{V,Cu2O} = 1.1 \times 10^{19}$ cm^{-3}, $E_{g,Cu2O} =$ 2.1 eV, $V_{bi} = 0.7$ V. Where ε_X is the dielectric constant, N_X is the carrier concentration, E_g is the bandgap, and V_{bi} is the built-in potential. In the diagrams E_C is the conduction band, E_V is the valence band, E_F is the fermi level, W_{ZnO} is the ZnO depletion width, and W_{Cu2O} is the copper oxide depletion width.

declining electric field distribution of the fully-ED reference cell. It is shown in Section 2.3 that because of the increased collection length, charges from long wavelengths (>460 nm) that are absorbed deep in the Cu_2O are more efficiently collected.

We also considered a bilayer ED-ZnO/AALD-Cu_2O^+ device with a Cu_2O^+ carrier density of 8.3×10^{15} cm^{-3} which would only require a Cu_2O^+ thickness of ~250 nm (i.e., ~1/4 of the collection length of ED Cu_2O) to produce the full built-in potential. However, all such ED-ZnO/AALD-Cu_2O^+ devices produced thus far showed little rectification which we believe to be due to the much smaller grain size of the AALD Cu_2O layer (~50 nm compared to ~1 µm in the ED Cu_2O), as seen in Figure 1. Thus, by adding the small crystals at the heterojunction interface, the density of grain boundaries and interface states increases dramatically. Such states act as recombination centers, deteriorating the performance of the ED-ZnO/AALD-Cu_2O^+ cell. On the other hand, in the BSF cell design, the high density of grain boundaries found in the Cu_2O^+ layer is isolated from the pn heterojunction. Fewer minority carriers (electrons) reach the Cu_2O^+ layer, and thus recombination due to the large number of grain boundaries is not as significant.

2.2. Improved Photovoltaic Performance with the Use of AALD Cu_2O^+

In this section, we present the experimental results of AALD-enhanced solar cells with various thicknesses of AALD Cu_2O^+ layers in comparison to a 3 µm and 1 µm fully-ED reference cell. A summary of the basic photovoltaic device parameters for 18 AALD-enhanced cells with different Cu_2O^+ thicknesses are presented in **Figure 3**. The thicknesses in Figure 3 are nominal values based on the deposition rate (1.25 nm min^{-1}) measured by correlating the number of deposition cycles to thicknesses of selected samples determined from cross section SEM images.

As seen from Figure 3a, the V_{OC} increases gradually with AALD Cu_2O^+ thickness while the spread in the data decreases with thickness. We predicted in Section 2.1 that ~150 nm of AALD Cu_2O^+ is necessary to replace the final 2 µm of the 3 µm reference cell for the same built-in potential. However, Figure 3a shows that a thickness closer to ~200 nm is needed to obtain the maximum V_{OC} of 0.32 V which is likely due to the fact that the shunt resistance is not sufficiently high for the full effect of the BSF to be attained until the AALD thickness is > 150 nm. The variability in the V_{OC} is also reduced for thicker AALD layers as more shunt pathways become covered. The maximum V_{OC} (0.32 V) was less than the value of the 3 µm reference cell (0.36 ± 0.03 V), likely due to recombination effects at the p-p$^+$ interface introduced by the AALD-enhanced design.

Figure 3b shows that J_{SC} improves with AALD thickness up to ~200 nm. Even a thin (~75 nm) AALD layer gives a 20% improvement in the average J_{SC} compared to the 1 µm reference cell. The J_{SC} of the best performing AALD-enhanced cell (~200 nm AALD Cu_2O^+ layer) gives a J_{SC} equal to 6.32 mA cm^{-2} which surpasses the J_{SC} of the 3 µm ED reference cell by 38% and the 1 µm ED reference cell by 50%. This value exceeds the performance of all previously reported cells produced under ambient conditions (tested under standard AM1.5 conditions)[5,7,8,10] and even approaches values (6.78 mA cm^{-2}) obtained for high

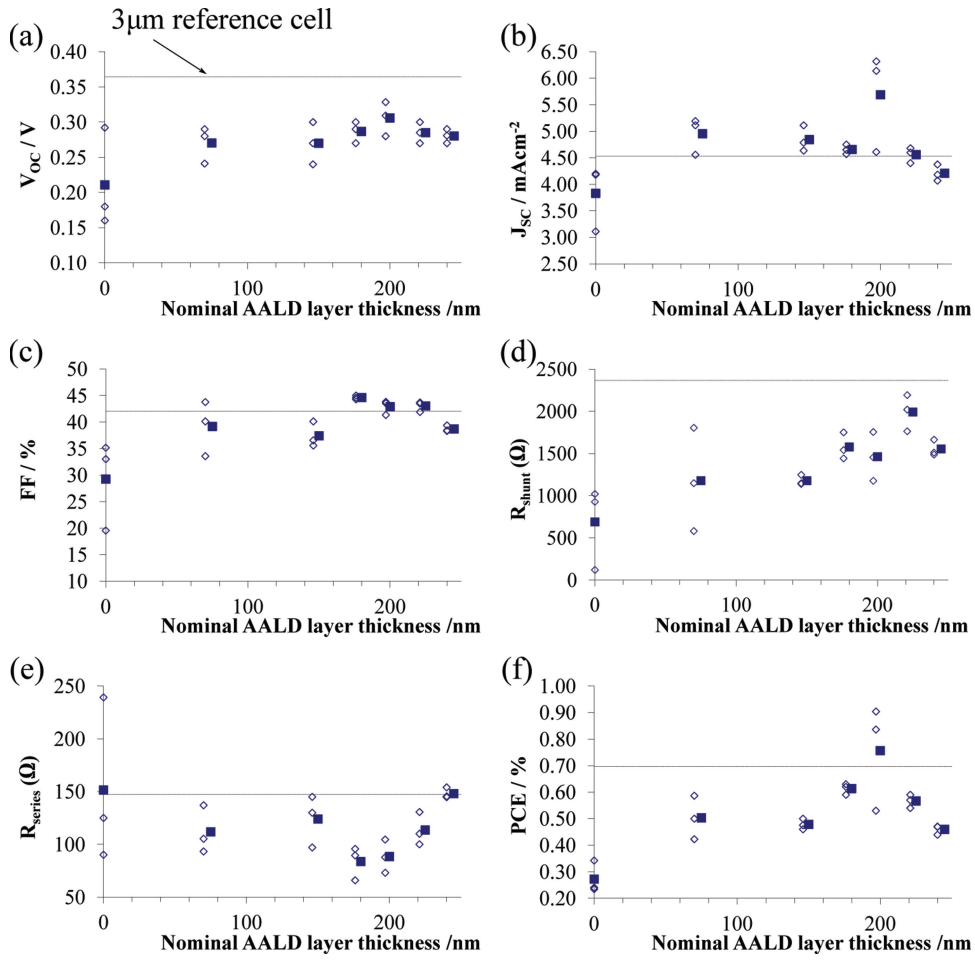

Figure 3. a) Open circuit voltage (V_{OC}), b) short circuit current density (J_{SC}), c) fill factor (FF), d) shunt resistance (R_{shunt}), e) series resistance (R_{series}), and f) power conversion efficiency (PCE). The dashed line (—) represents the performance of an average of three 3-μm Cu_2O reference cells. The 1-μm Cu_2O reference cells data is shown as data points at 0 nm AALD layer thickness. The closed squares (■) represent the average of 3 data measurements, shown by the open dimonds (◊), for each AALD thickness. Nominal thickness is based on the Cu_2O^+ growth rate calibrated for selected samples by cross section SEM with the number of deposition cycles.

temperature, vacuum deposited cells.[4] The occurrence of the maximum J_{SC} at ~200 nm is consistent with the peak in V_{OC} (and therefore maximum electric field) at the same thickness (Figure 3a). Since the majority of the device exists within the depletion region, charge collection is mainly drift limited. Thus potential and therefore electric field enhancements will have a major benefit to the collection efficiency.

In a previous investigation for the same ED-ZnO/ED-Cu_2O(1 μm) system,[5] we showed that an electrically-neutral blocking layer between the ED Cu_2O and the back electrode can help prevent shunting but provides little enhancement to the J_{SC}. In this investigation, however, a large increase in the J_{SC} is observed for the AALD-enhanced design which corroborates our claim that the Cu_2O^+ layer builds in a strong field increasing the collection efficiency of the device. We discuss the improved collection efficiency in more detail in the next section.

Figure 3c shows a trend of increasing FF with Cu_2O^+ thickness. At ~175 nm of Cu_2O^+, the FF reaches values of 38.7–45.0% which are equivalent to the average FF (± 1 standard deviation) value of the 3 μm reference cell (42 ± 3.2%) and are ~45% higher than the average 1 μm reference cell. FF is dependent upon the shunt resistance and series resistance of the device.

The shunt resistance (Figure 3d) strongly correlates with AALD thickness since thicker AALD layers make conduction through leakage pathways more difficult. In addition, for thicker AALD layers a larger electric field is built across the device preventing recombination at defect states which can also reduce the shunt resistance.

The series resistance shows no clear trend with AALD thickness (Figure 3e) consistent with the AALD layer having a high carrier concentration thus contributing little to the overall cell resistance. The values are all observed to be lower than those of both the 3 μm reference and 1 μm reference cells. AFM (not shown) indicates that the AALD layer creates a smoother surface which allows for better contact with the back electrode and therefore reduces the series resistance.

Figure 3f shows an increasing PCE with AALD thickness which correlates closely with the J_{SC}. The best performing cell showed a 28% increase in overall device efficiency (reaching 0.90%) compared to the 3 μm reference cell. The high

efficiency achieved for this class of atmospherically processed device is slightly lower than a fully-ED device reported by Izaki et al.[7] which had an efficiency of 1.2% and a large V_{OC} (0.56 V). The high V_{OC} is indicative of a more perfect interface and less recombination in their device, although it is unclear how such a result was obtained since in low temperature electrochemically processed materials, high defect concentrations are commonplace. Nonetheless, our AALD-enhanced cell had a J_{SC} that was 66% higher due to the novel optimization of the collection length and device thickness. For AALD layers thicker than 200 nm, the PCE is observed to decrease marginally. We speculate that this is because of a decrease in charge collection efficiency for layers thicker than the depletion region since charge collection in this region is diffusion limited. Hence, light that was previously reflected off the back electrode and collected within the depletion region will now be absorbed in the neutral region and likely remain uncollected due to a low minority carrier mobility in the absence of an electric field.

2.3. Improved Charge Collection: EQE Studies

Figure 4 shows the EQE spectra of the best performing thin (~75 nm) and thick (~200 nm) AALD-enhanced cells in comparison to the fully-ED 1 µm and 3 µm reference cells. We study these thicknesses to demonstrate that (a) for thin AALD layers the collection efficiency is improved compared to the 1 µm reference cell, and (b) AALD layers around the optimum thickness (~200 nm) give improved charge collection that surpass both the 1 µm and 3 µm reference cells. We propose that the high J_{SC} and high collection efficiency results from a combination of 3 factors: (1) the strong BSF effect from the p^+ layer which improves charge extraction, (2) reduction of total Cu_2O thickness to approximately the charge collection length and (3) enhanced collection of charges from light reflecting off the back electrode. These improvements can be identified from two wavelength regions of the EQE spectrum discussed below.

EQE at middle wavelengths (375 nm–460 nm): In this wavelength region, the average EQE is increased from 72% for the fully-ED 3 µm reference cell to 85% for the ~200 nm AALD-enhanced cell. In Cu_2O, photons with wavelengths between 375 nm and 460 nm have optical depths of 0.4 µm or less.[9,43] Hence, in the 3 µm reference cell holes need to travel through 2.6 µm of a resistive Cu_2O layer to the metal contact resulting in recombination with photogenerated electrons. By contrast, in the ~200 nm AALD-enhanced cell, the BSF builds in a strong electric field to drive carriers out of the device. In addition, the 2 µm recombination region of the fully-ED cell is eliminated, thus drastically reducing the number of 'lost' carriers and strongly increasing the EQE. The ~75 nm AALD -enhanced cell also exhibits a 45% higher EQE compared to the 1 µm-Cu_2O reference cell, confirming that even a thin AALD layer increases the electric field, consistent with the modelling shown in Figure 2 and with the J_{SC} plot in Figure 3b.

EQE at long wavelengths (> 460 nm): As shown by Figure 4a, the collection of the longer wavelength light (>460 nm) is higher for the ~200 nm AALD-enhanced sample compared to the 3 µm reference cell despite the fact that most of the light in this wavelength region is 'absorbed' at distances >1 µm in

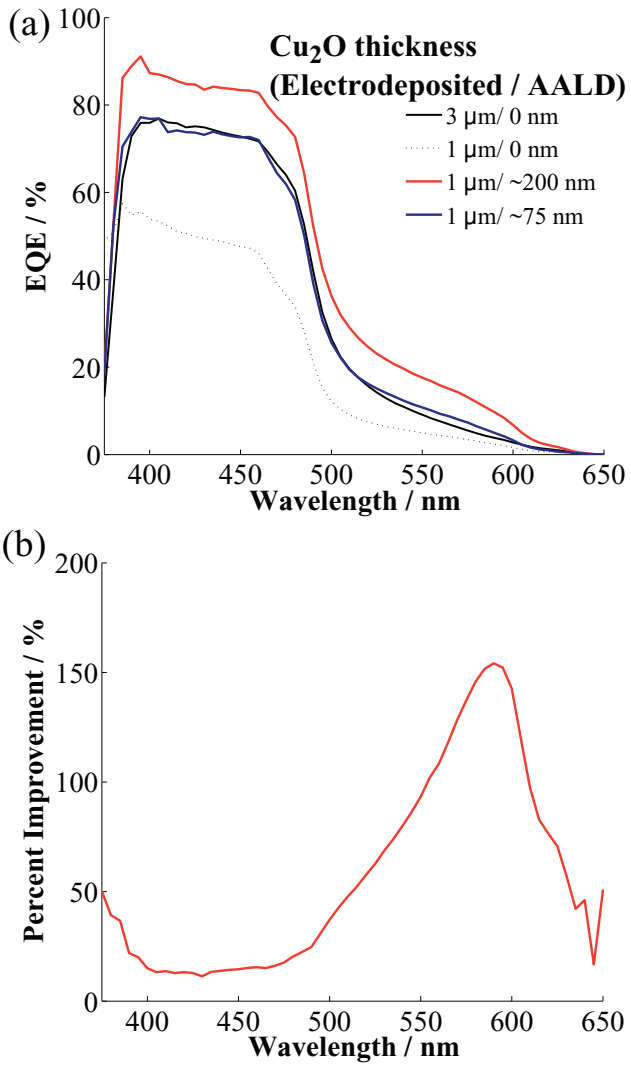

Figure 4. a) EQE spectra of a thin (~75 nm) and thick (~200 nm) AALD-enhanced cell ($ZnO/Cu_2O/Cu_2O^+$) compared to a 1 µm-Cu_2O and 3 µm-Cu_2O fully-ED (ZnO/Cu_2O) cell. b) Percent EQE improvement as a function of wavelength of the thick AALD-enhanced cell versus the 3 µm fully ED reference cell.

Cu_2O (i.e. distances larger than the approximate thickness of the AALD-enhanced sample).[9] As has been noticed by our group previously,[5] when the Cu_2O layer thickness is reduced to ~1 µm, unabsorbed incident light reflects off the back electrode. This light can then be absorbed on a second pass through the device at a location within the collection region, thus allowing improved minority carrier collection for these wavelengths and a higher percent improvement (up to 150% - Figure 4b) than the medium wavelength region. For the ~200 nm AALD-enhanced sample, the strong electric field further supplements the collection of charges in this region.

Similar to the middle wavelength region, for wavelengths > 460 nm the ~75 nm AALD sample shows an improved EQE compared to the 1 µm reference cell, in agreement with Figure 3b. Since similar reflection-enhanced absorption profiles are expected for both of these samples, the data emphasises the

effects of both increased electric field from the BSF effect and the closing of shunt pathways, which together allow more of the charges from the reflected light to be collected.

3. Conclusions

In low temperature, atmospherically grown ZnO/Cu_2O solar cells, the discrepancy between the low charge collection length (<1 μm) and large depletion width (up to 3 μm) in the Cu_2O was addressed. Two different atmospheric chemical growth techniques were combined to optimize cell performance. It was possible to considerably improve the efficiency of the cell by using an ED Cu_2O layer of only 1 μm coated with a <200 nm overlayer of Cu_2O^+ grown by atmospheric atomic layer deposition, rather than a standard 3 μm ED Cu_2O film. Using this structure, we achieved a device efficiency of 0.90% (a 28% improvement compared to a fully-ED cell) and obtained the highest reported J_{SC} of 6.32 mA cm^{-2} for this system grown under atmospheric conditions. The ZnO/Cu_2O/Cu_2O^+ design was made possible by the 100-fold increase in hole concentration of the AALD Cu_2O^+ overlayer which allowed the depletion width to be obtained in a total cell thickness commensurate with the minority carrier collection length. Modelling confirmed that the new design increased the electric field and charge collection throughout the cell. A reduced total thickness of our cells has the added benefit that the number of charges lost to recombination is reduced and that light which is reflected off the back electrode can be absorbed within the collection region. Finally, the conformality and high density of the AALD Cu_2O^+ film reduces shunt pathways in the underlying ED Cu_2O layer.

4. Experimental Section

Indium Tin Oxide (ITO) substrates (14 mm x 14 mm x 0.7 mm, sheet resistance < 10 Ω sq^{-1}) were commercially purchased from Praezisions Glas & Optik. Substrates were cleaned in an ultrasonic bath in water, acetone, and isopropanol for 15 minutes each. All chemicals were reagent grade and the water was purified to a resistivity greater than 16 MΩ cm.

A Princeton Applied Research Model 363 Potentiostat/Galvanostat was used to supply a constant voltage or current for the depositions. ZnO films were grown on the ITO via potentiostatic deposition at −0.85 V vs a Ag/AgCl (saturated KCl) reference electrode,[44] at a temperature 74 ± 1 °C. The solution used was $Zn(NO_3)_2$ (0.08 M) with 15% volume ethanol added to give dense films without pinholes.[45] Fresh solution was used for each deposition and all films were grown to an approximate thickness of 500 nm.

Cu_2O was deposited galvanostatically onto the ZnO film at −1.0 mA cm^{-2} from an aqueous solution of Cu_2SO_4(0.4 M)/ lactic acid (3 M) at 40 °C.[7] The pH was adjusted to 12.6 by adding NaOH (4 M).

For the AALD reactor, a shower-head simultaneously delivers vaporized chemical precursors to the substrate below, which sits on a heated platen moving back and forth under the head. An inert gas is passed through the chemical lines to control the flow rate and spacing between the precursors, thereby controlling the chemical reaction, reaction regime (i.e. ALD vs chemical vapor deposition), and deposition rate. Additional descriptions of atmospheric ALD equipment are available elsewhere,[30–35] including our specific approach.[33]

For this investigation, the AALD Cu_2O^+ layer was deposited using a Cupraselect metal precursor heated to 65 °C. Water was used as the oxygen precursor and N_2 was used as the inert gas. The flow rates for the three gases were 500 mL min^{-1} for Cupraselect, 50 mL min^{-1} for H_2O, and 1000 mL min^{-1} for N_2. The temperature of the platen holding the substrate was set to 150 °C and the speed of the platen movement back and forth under the AALD shower head was 50 mm s^{-1}. Various thicknesses of AALD Cu_2O^+ (~75–250 nm) were deposited onto the 1 μm ED Cu_2O layer. The film growth rate was ~1.25 nm min^{-1} as determined from fitting measured thickness to the number of deposition cycles. Gold contacts were evaporated on the Cu_2O using a BOC Edwards Auto 306 resistance evaporator.

The carrier concentrations of the Cu_2O and Cu_2O^+ films were determined from Hall Effect measurements using a Keithley 6221 current source, Keithley 182 Nanovoltmeter, and a home built differential electrometer with input resistance of 1×10^{14} Ω. Samples were measured in the van der Pauw configuration. For the ED Cu_2O, prior to the Hall measurements the film was transferred from the ITO to a non-conducting substrate (glass) using an epoxy liftoff technique.[46]

Film thicknesses were measured using cross section scanning electron microscopy (SEM) images taken using a LEO VP-1530 field emission SEM. RMS roughness was calculated from Atomic Force Microscopy (AFM) scans using a Bruker Multimode Nanoscope III.

J–V measurements were performed at 100 mW cm^{-2} using an AM1.5 ABET class AAA solar simulator calibrated with a silicon reference diode and corrected for spectral mismatch. R_{shunt} was calculated from the slope of the JV curve in reverse bias, 0.1 V before the J_{SC}, and R_{series} was calculated from the slope of the *J–V* curve, 0.1 V after the V_{OC}. A monochromator with a 100 W tungsten halogen lamp was used to measure the EQE.

Equations for the electric field of the p-p^+ junction were solved using the PC1D modeling software.[40] For the model, 3 regions were used to simulate the ZnO, the Cu_2O, and Cu_2O^+ regions of the device. For the Cu_2O^+ region, the thickness was set longer than necessary and the depletion width was estimated as the location that the electric field approached 0 V cm^{-1}.

Supporting Information

Supporting Information is available from the Wiley Online Library or from the author.

Acknowledgements

The authors would like to acknowledge the International Copper Association, the ERC for the Advanced Investigator Grant, Novox, ERC-2009-adG 247276, the Gates Cambridge Trust, and Girton College (Cambridge) for funding this work. D.M.R. acknowledges funding from ERC's Marie Curie program (FP7/2007–2013, grant agreement number 219332) and the Comissionat per a Universitats i Recerca (CUR) del DIUE de la Generalitat de Catalunya.

Received: November 5, 2012
Published online: February 6, 2013

[1] C. Wadia, A. P. Alivisatos, D. M. Kammen, *Env. Sci. Technol.* **2009**, *43*, 2072.
[2] K. P. Musselman, L. Schmidt-Mende, *Green* **2011**, *1*, 7.
[3] S. Jeong, A. Mittiga, E. Salza, A. Masci, S. Passerini, *Electrochim. Acta* **2008**, *53*, 2226.
[4] A. Mittiga, E. Salza, F. Sarto, M. Tucci, R. Vasanthi, *Appl. Phys. Lett.* **2006**, *88*, 163502.
[5] T. Gershon, K. P. Musselman, A. Marin, R. H. Friend, J. L. MacManus-Driscoll, *Sol. Energy Mater. Sol., C.* **2012**, *96*, 148.
[6] J. Katayama, K. Ito, M. Matsuoka, J. Tamaki, *J. Appl. Electrochem.* **2004**, *34*, 687.

[7] M. Izaki, T. Shinagawa, K. T. Mizuno, Y. Ida, M. Inaba, A. Tasaka, *J. Phys. D: Appl. Phys.* **2007**, *40*, 3326.
[8] K. P. Musselman, A. Marin, A. Wisnet, C. Scheu, J. L. MacManus-Driscoll, L. Schmidt-Mende, *Adv. Funct. Mater.* **2011**, *21*, 5.
[9] K. P. Musselman, *PhD Thesis*, University of Cambridge, UK **2010**.
[10] K. P. Musselman, A. Marin, L. Schmidt-Mende, J. L. MacManus-Driscoll, *Adv. Funct. Mater.* **2012**, *22*, 2202.
[11] K. P. Musselman, A. Wisnet, D. C. Iza, H. C. Hesse, C. Scheu, J. L. MacManus-Driscoll, L. Schmidt-Mende, *Adv. Mater.* **2010**, *22*, E254.
[12] Y. Liu, H. K. Turley, J. R. Tumbleston, E. T. Samulski, R. Lopez, *Appl. Phys. Lett.* **2011**, *98*, 162105.
[13] E. Yablonovitch, G. D. Cody, *IEEE T. Electron Dev.* **1982**, *29*, 300.
[14] A. Usami. *Sol. Energy Mater. Sol. C.* **2000**, *64*, *75*.
[15] R. J. Elliott, *Phys. Rev.* **2007**, *108*, 1384.
[16] P. W. Baumeister, *Phys. Rev.* **1961**, *121*, 359.
[17] S. Ishizuka, S. Kato, T. Maruyama, K. Akimoto, *Jpn. J. Appl. Phys.* **2001**, *40*, 2765.
[18] S. Ishizuka, S. Kato, Y. Okamoto, K. Akimoto, *J. Cryst. Growth* **2002**, *237*, 616.
[19] S. Suzuki, T. Miyata, T. Minami, *J. Vac. Sci. Technol., A* **2003**, *21*, 1336.
[20] S. Ishizuka, K. Akimoto, *Appl. Phys. Lett.* **2004**, *85*, 4920.
[21] N. Kikuchi, K. Tonooka, *Thin Solid Films* **2005**, *486*, 33.
[22] K. Akimoto, S. Ishizuka, M. Yanagita, Y. Nawa, G. K. Paul, T. Sakurai, *Sol. Energy* **2006**, *80*, 715.
[23] B. S. Li, K. Akimoto, A. Shen, *J. Cryst. Growth* **2009**, *311*, 1102.
[24] C. T. Sah, F. A. Lindholm, J. G. Fossum, *IEEE Trans. Electron Dev.* **1978**, *25*, 66.
[25] J. Fossum, R. Nasby, S. Pao, *IEEE Trans. Electron Dev.* **1980**, *27*, 785.
[26] J. Mandelkorn, J. H. Lamneck Jr., *Sol. Cells* **1990**, *29*, 121.
[27] M. P. Godlewski, C. R. Baraona, H. W. Brandhorst Jr., *Sol. Cells* **1990**, *29*, 131.
[28] Z. T. Kuznicki, *Sol. Energy Mater. Sol. C.* **1993**, *31*, 383.
[29] L. Zhu, G. Shao, J. K. Luo, *Semicond. Sci. Technol.* **2011**, *26*, 085026.
[30] D. H. Levy, S. F. Nelson, D. Freeman, *J. Disp. Technol.* **2009**, *5*, 484.
[31] P. Poodt, V. Tiba, F. Werner, J. Schmidt, A. Vermeer, F. Roozeboom, *J. Electrochem. Soc.* **2011**, *158*, H937.
[32] P. Poodt, A. Lankhorst, F. Roozeboom, K. Spee, D. Maas, A. Vermeer, *Adv. Mater.* **2010**, *22*, 3564.
[33] L. Dunlop, A. Kursumovic, J. L. MacManus-Driscoll, *Appl. Phys Lett.* **2008**, *93*, 172111.
[34] F. Werner, B. Veith, V. Tiba, P. Poodt, F. Roozeboom, R. Brendel, J. Schmidt, *Appl. Phys. Lett.* **2010**, *97*, 162103.
[35] F. Werner, W. Stals, R. Görtzen, B. Veith, R. Brendel, J. Schmidt, *Energy Procedia* **2011**, *8*, 301.
[36] Y. Hishikawa, E. Maruyama, S. Yata, M. Tanaka, S. Kiyama, S. Tsuda, *Sol. Energy Mater. Sol. C.* **1997**, *49*, 143.
[37] S. Hore, C. Vetter, R. Kern, H. Smit, A. Hinsch. *Sol. Energy Mater Sol. C.* **2006**, *90*, 1176.
[38] K. Tvingstedt, V. Andersson, F. Zhang, O. Inganäs, *Appl. Phys. Lett.* **2007**, *91*, 123514.
[39] M. Ichimura, Y. Song, *Jpn. J. Appl. Phys.* **2011**, *50*, 051002.
[40] D. A. Clugston, P. A. Basore, *26th IEEE Photovoltiac Specialists Conference* **1997**, 207.
[41] Z. T. Kuznicki, *J. Appl. Phys.* **1991**, *69*, 6526.
[42] A. V. Shah, H. Schade, M. Vanecek, J. Meier, E. Vallat-Sauvain, N. Wyrsch, U. Kroll, C. Droz, J. Bailat, *Prog. Photovoltaics: Res. Appl.* **2004**, *12*, 113.
[43] L. C. Olsen, F. W. Addis, W. Miller. *Sol. Cells* **1982**, *7*, 247.
[44] M. Izaki, T. Omi, *Appl. Phys. Lett.* **1996**, *68*, 2439.
[45] K. P. Musselman, T. Gershon, L. Schmidt-Mende, J. L. MacManus-Driscoll, *Electrochim. Acta* **2011**, *56*, 3758.
[46] M. Miyake, K. Murase, T. Hirato, Y. Awakuraz, *J. Electrochem. Soc.* **2003**, *150*, C413.